Tuning of coupling modes in laterally parallel double open quantum dots

Chi-Shung Tang,[1] Wing Wa Yu,[2] and Vidar Gudmundsson[2]
[1]*Physics Division, National Center for Theoretical Sciences, P.O. Box 2-131, Hsinchu 30013, Taiwan*
[2]*Science Institute, University of Iceland, Dunhaga 3, IS-107 Reykjavik, Iceland*
(Received 29 July 2005; revised manuscript received 30 September 2005; published 21 November 2005)

We consider electronic transport through laterally parallel double open quantum dots embedded in a quantum wire in a perpendicular magnetic field. The coupling modes of the dots are tunable by adjusting the strength of a central barrier and the applied magnetic field. Probability density and electron current density are calculated to demonstrate transport effects including magnetic blocking, magnetic turbulence, and a holelike quasibound state feature. Fano to dip line-shape crossover in the conductance is found by varying the magnetic field.

DOI: 10.1103/PhysRevB.72.195331 PACS number(s): 73.23.−b, 73.21.La, 73.21.Hb, 85.35.Ds

I. INTRODUCTION

Electronic transport through an open quantum dot has attracted broad attention[1–12] due to its potential in the investigation of various bound-state features,[8] phase coherence,[9,10] and wave function imaging.[11,12] In high electron mobility samples at low temperatures, the electron phase coherent length may be longer than the dimension of the open dot system, allowing electrons to remain coherent while traversing the system with negligible impurity effects. Moreover, since the outgoing electrons from the open dot are strongly coupled to reservoirs without tunneling, the Coulomb effects are negligible.

By coupling two quantum dots in series or in parallel, a double quantum dot is formed.[13–16] Quantum transport through such a double dot system has attracted considerable attention due to its versatility for various applications.[17–30] The double dot system provides a possible new mechanism compared to a single quantum dot as electrons could be coupled between the two dots, thus forming an artificial quantum dot molecular junction.[17–20] In addition, the coupled dot system is likely to be important in the study of magnetoconductance fluctuations,[21] dephasing properties,[22,23] and quantum information processing,[24–27] where external field manipulation and quantum coherence are both required. Thus far these coupled dot systems are, however, assumed to be isolated and can be described by an Anderson-type model.[28–30]

We would like to emphasize that the adiabaticity of the dot-lead connection holds only for large quantum dots. As the dot size shrinks and approaches the realm of the Fermi wavelength, the dot-lead connection no longer remains adiabatic. Experimental findings in electronic transport through quantum dots, such as the individual eigenstates of an isolated dot[31] and the recurrence of specific groups of wave function scars in the dot,[6] indicate unequivocally the mode-mixed scattering at the dot-lead connections. It has been shown that the embedded quantum structures can lead to a complicated mode mixing.[32,33]

In this paper we study the tuning of coupling modes of parallel double open quantum dots (DOQDs) embedded in a quantum wire. The mode-coupling in this system is coherently adjusted by a central elongated potential barrier separating the system into upper and lower channels, as depicted in Fig. 1. In addition, an external perpendicular magnetic field is applied to manipulate the electronic cyclotron motion and the coupling between the upper dot (UD) and the lower dot (LD). It is important to note that since the DOQD system is strongly coupled to the source and drain reservoirs, the quantum interference effects are strong and cannot be treated like an isolated dot using an Anderson-type model or solving the rate equation for the Fock-Darwin spectrum.[34] Here we employ the Lippmann-Schwinger approach[32,33] that allows us to handle a wide range of smooth scatterers embedded in a wire and access the electron probability distribution as well as the electron current flow in the system.

One robust transport phenomenon in open quantum structures is the quasibound-state feature with positive[35,36] or negative[37,38] binding energy. Indeed, the transport properties of a wire with either static or time-dependent scatters can exhibit significant quasibound-state features.[35–39] In a laterally parallel DOQD system, operating the central barrier simultaneously adjusts the dot-dot and dot-lead coupling and tilts the potential of the side dots to affect the alignment of the electron energy with the discrete levels in the dots. The

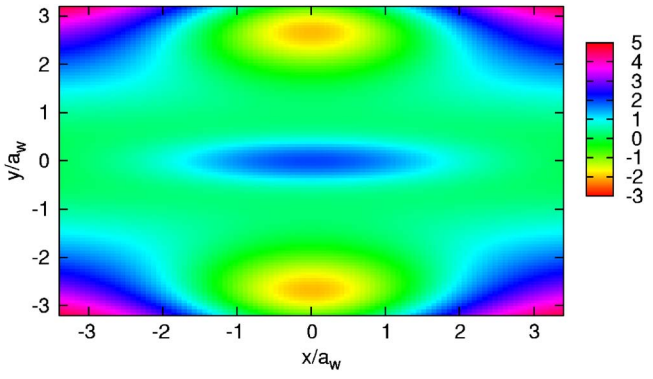

FIG. 1. (Color online) Top-view schematic illustration of the laterally parallel DOQD system containing two open quantum dots (yellow) to the sides and a central barrier (blue). The color scale on the right shows the potential height in meV. The parameters are a_w=33.7 nm, $\hbar\Omega_0$=1.0 meV, $V_1=V_3=-6.0$ meV, and V_2=2.0 meV.

electronic transport thus manifests different types of resonant features.

II. MODEL: A LIPPMANN-SCHWINGER APPROACH

The system under investigation is composed of a laterally parallel DOQD embedded in a quantum wire with confining potential $V_c(y)=\frac{1}{2}m^*\Omega_0^2y^2$, and hence the electrons are transported through the wire with characteristic energy scale $\hbar\Omega_0$ in the transverse direction. The parallel double open quantum dots are separated by a central barrier that can be used to tune the dot coupling and adjust the mode mixing between the wire subbands and the dot levels. The electrons incident from the left reservoir impinge on the parallel DOQD system modeled by the Gaussian-type scattering potential

$$V_{sc}(x,y)=\sum_{i=1}^{3} V_i \exp[-\alpha x^2-\beta_i(y-y_i)^2]. \tag{1}$$

Here V_1 and V_3 are negative indicating, respectively, the depth of the UD and the LD, and V_2 is positive describing the height of the central barrier. The three potentials have the same length (same α) while the central barrier is a little narrower then the two dots ($\beta_1=\beta_3<\beta_2$) so that the UD is allowed to couple with the LD. In a perpendicular magnetic field $\mathbf{B}=B\hat{\mathbf{z}}$, the parabolic confinement defines an effective magnetic length $a_w=(\hbar/m^*\Omega_w)^{1/2}$ in the wire. In the presence of a magnetic field, the quantized electron energy away from the parallel DOQD system is given by[40]

$$E_n(k)=\left(n+\frac{1}{2}\right)\hbar\Omega_w+\frac{(ka_w)^2}{2}\frac{(\hbar\Omega_0)^2}{\hbar\Omega_w}, \tag{2}$$

where k is the magnitude of the electron wave vector along the wire and $n=0,1,\ldots$. This defines the effective subband separation $\hbar\Omega_w$, where $\Omega_w^2=\omega_c^2+\Omega_0^2$ is related to the cyclotron frequency $\omega_c=eB/(m^*c)$ and the characteristic frequency Ω_0 for the parabolically confined wire away from the parallel DOQD system. We assume a value of $m^*=0.067m$ for the effective mass of an electron in GaAs-based material.

In the following we employ a mixed momentum-coordinate presentation[41]

$$\Psi_E(p,y)\equiv\int dx e^{-ipx}\psi_E(x,y) \tag{3}$$

and utilize a channel-mode expansion $\Psi_E(p,y)=\Sigma_n\varphi_n(p)\phi_n(p,y)$ to obtain a set of coupled Lippmann-Schwinger integral equations in the momentum space. As such, these equations can then be transformed into integral equations for the T-matrix to facilitate numerical calculation.[32] According to the Landauer-Büttiker formalism the energy dependence of the conductance can be calculated as[32]

$$G(E)=G_0\,\mathrm{Tr}[\mathbf{t}^\dagger(E)\mathbf{t}(E)] \tag{4}$$

with the conductance quantum $G_0=2e^2/h$. Furthermore, with the scattering wave function obtained from the T-matrix we calculate in configuration space the probability density $|\psi_E(x,y)|^2$ and the electron current density

$$\mathbf{J}=\frac{e}{m}\,\mathrm{Re}\left[\psi_E^*\left(\mathbf{p}+\frac{e}{c}\mathbf{A}\right)\psi_E\right] \tag{5}$$

to clearly demonstrate the transport mechanism and provide detailed insight into the coupling nature of the parallel DOQD system. Here $-e$ is the charge of an electron. For embedded wire systems it is convenient to choose the vector potential $\mathbf{A}=(-By,0,0)$ in a Landau gauge.

III. RESULTS AND DISCUSSION

To study the transport behavior in a laterally parallel DOQD system, we consider a broad parabolic wire with confinement energy $\hbar\Omega_0=1.0$ meV. This energy corresponds to $a_w=33.7$ nm in zero magnetic field. In the DOQD system, the central barrier and the side dots have the same effective length $L\simeq 141$ nm ($\alpha=2\times10^{-4}$ mm^{-2}), while the width of the central barrier ($\beta_2=4\times10^{-3}$ mm^{-2}) is narrower than the side dots ($\beta_1=\beta_3=0.7\times10^{-3}$ mm^{-2}) to facilitate the UD-LD coupling. By choosing these parameters, the effective width of the central barrier and the side dots are, respectively, $W_{CB}\simeq 32$ nm and $W_{SD}\simeq 76$ nm. The two open dots have the same potential depth $V_1=V_3=-6.0$ meV and are separated by 100 nm from the central barrier ($y_2=0$), namely, $y_1=-y_3=100$ nm.

In performing the numerical calculation, a sufficient total number of quantum channels including evanescent modes in momentum space is needed to satisfy the conservation of the current condition. Numerical accuracy is assured by comparing the data obtained from a larger basis set. In order to investigate the characteristics of the energy-dependent conductance $G(E)$ by tuning the strength of a central barrier and the applied magnetic field, below we show the conductance as a function of

$$X=\frac{E}{\hbar\Omega_w}+\frac{1}{2}. \tag{6}$$

The integer part of the parameter X counts how many propagating channels in the wire are open for an incoming electron with energy E.

A. Tuning the central barrier

In Fig. 2, we investigate the tuning effects of the central barrier V_2 in a magnetic field $B=0.5$ T. Correspondingly, the effective magnetic length $a_w=29.34$ nm and the effective subband separation $\hbar\Omega_w=1.32$ meV, and hence $a_w=a_{2D}\sqrt{\omega_c/\Omega_w}\simeq 0.8a_{2D}$ with a_{2D} being the magnetic length in a flat two-dimensional system. The center of the side dots are located at $(x_c,y_c)=(0,\pm 3.4a_w)$. The magnetic field at 0.5 T provides an optimal length scale fitting to the size of the parallel DOQD system. In the single-mode ($1<X<2$) regime, the magnetic field enhances the conductance in the low kinetic energy (KE) regime. Contrarily, in the high KE regime, the electron essentially becomes pinned around the central barrier and hence the conductance is strongly suppressed manifesting a *magnetic blocking effect*. In the double-mode regime ($2<X<3$), this blocking effect is suppressed due to the enhanced mode-mixing resonance with

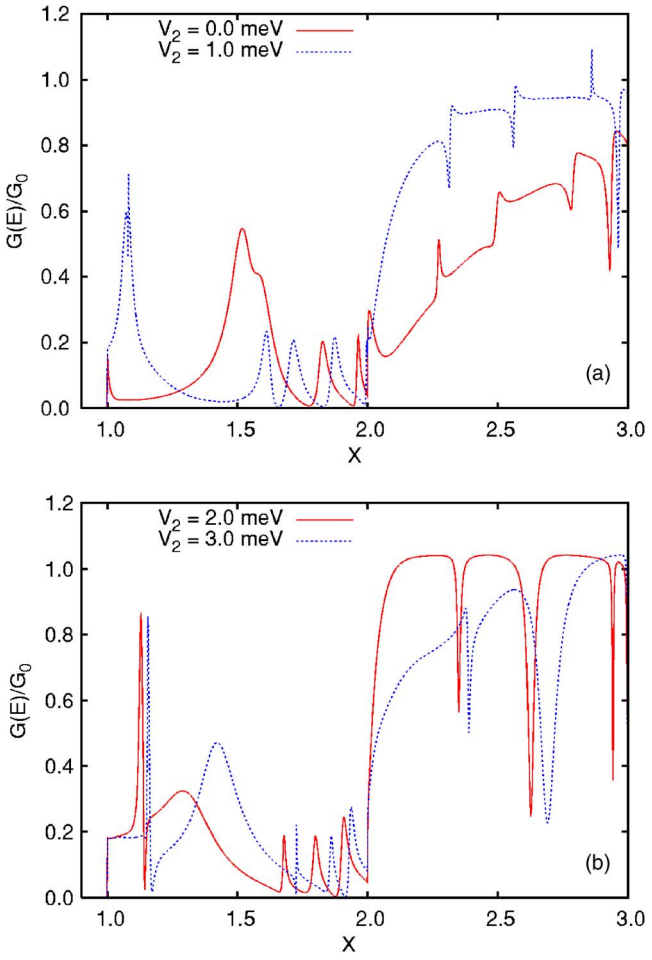

FIG. 2. (Color online) The conductance in units of $G_0=2e^2/h$ as a function of X in a magnetic field $B=0.5$ T with a different height of the central barrier $V_2=$(a) 0.0 (solid) and 1.0 (dashed) meV; and (b) 2.0 (solid) and 3.0 (dashed) meV. Other parameters are $V_1=V_3=-6.0$ meV and $L=4.82a_w$.

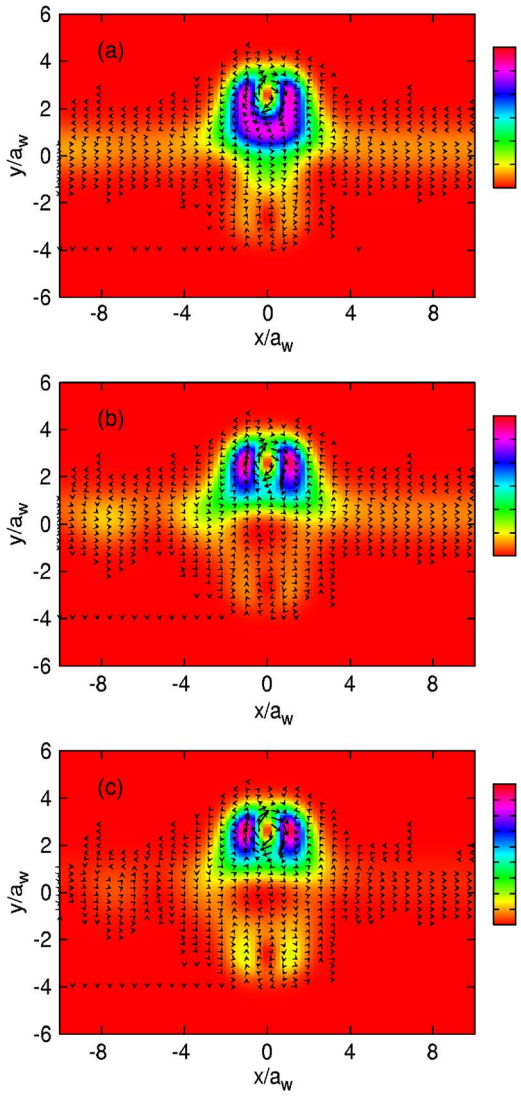

FIG. 3. (Color online) Probability density and electron current density (black arrows) are plotted as functions of x and y in a magnetic field $B=0.5$ T with different strength of the central barrier in the low-KE single-mode regime: (a) $V_2=1.0$ meV at $X=1.081$; (b) $V_2=2.0$ meV at $X=1.13$; and (c) $V_2=3.0$ meV at $X=1.16$. Other parameters are $V_1=V_3=-6.0$ meV and $L=4.82a_w$.

strong UD-LD coupling in the DOQD system. Moreover, in the double-mode regime, the conductance envelope manifests a plateaulike behavior ($G/G_0\approx 1.0$) indicating that the direct backscattering due to the central barrier is essentially suppressed.

1. Single-mode regime

In the low-KE single-mode regime, we find a Fano-type line shape[42] in G when the UD can be separated from the LD with the help of a central barrier, as is shown in Fig. 2. More precisely, the peaks of these Fano-type line shapes occur (i) at $X=1.081$ with $G/G_0=0.71$ for the case of $V_2=1.0$ meV; (ii) at $X=1.13$ with $G/G_0\approx 0.86$ for the case of $V_2=2.0$ meV; and (iii) at $X=1.16$ with $G/G_0\approx 0.84$ for the case of $V_2=3.0$ meV. These structures represent resonant transmission of electrons with continuous subband energy in the leads that strongly couple to the discrete level in the UD forming a long-lived quasibound state with quantum number $(n_x,n_y)=(1,2)$ in the UD.[8]

It is important to point out that the clockwise cyclotron motion in the UD indicates a magnetic field induced *holelike quasibound state* in the UD, as is shown in Figs. 3(a)–3(c). This is one of the key features in the present work. It is clearly demonstrated in Fig. 3(a) that the weak dip-and-peak structure Fano-type line shape, shown by the dashed curve in Fig. 2(a), is due to the weakness of the central barrier such that the electrons can still have significant coupling to the LD. In addition, these holelike quasibound states, exhibiting Fano structures in G, are shifted by changing V_2 because of the tilting effect to the potential configuration of the open dots by the central barrier.

When the central barrier is tuned to be higher, e.g., $V_2=2.0$ or 3.0 meV, the electrons can be confined longer to the UD forming a perfect (2,1)-like quasibound state in the UD [see Figs. 3(b) and 3(c)], and hence the conductance manifests a strong peak-and-dip line shape. We note in passing that there are Fano-type dips (i) at $X=1.079$ for V_2

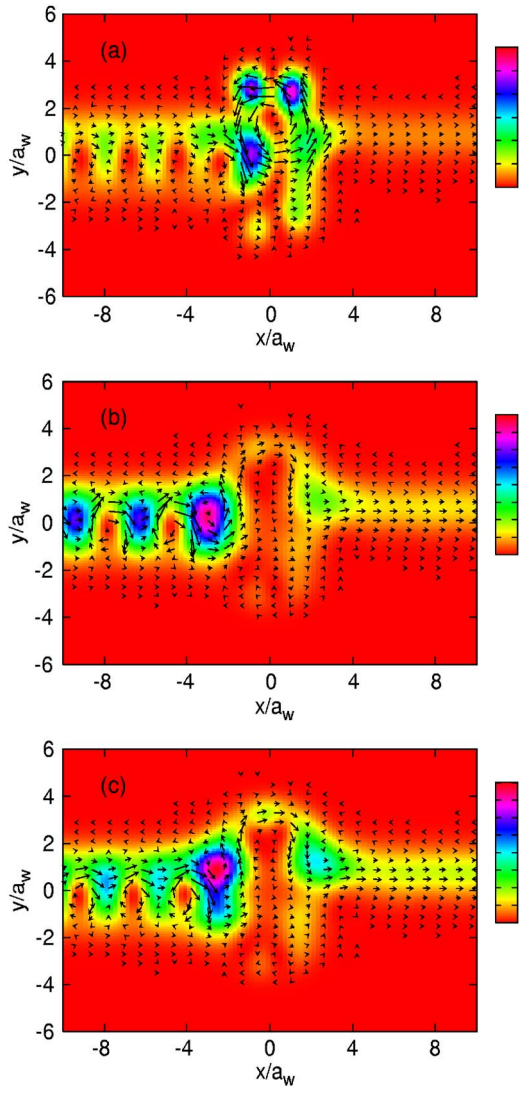

FIG. 4. (Color online) Probability density and electron current density (black arrows) are plotted as functions of x and y in a magnetic field $B=0.5$ T with different strength of the central barrier in the mediate-KE single-mode regime: (a) $V_2=0.0$ meV at $X=1.52$; (b) $V_2=2.0$ meV at $X=1.29$; and (c) $V_2=3.0$ meV at $X=1.42$. Other parameters are $V_1=V_3=-6.0$ meV and $L=4.82a_w$.

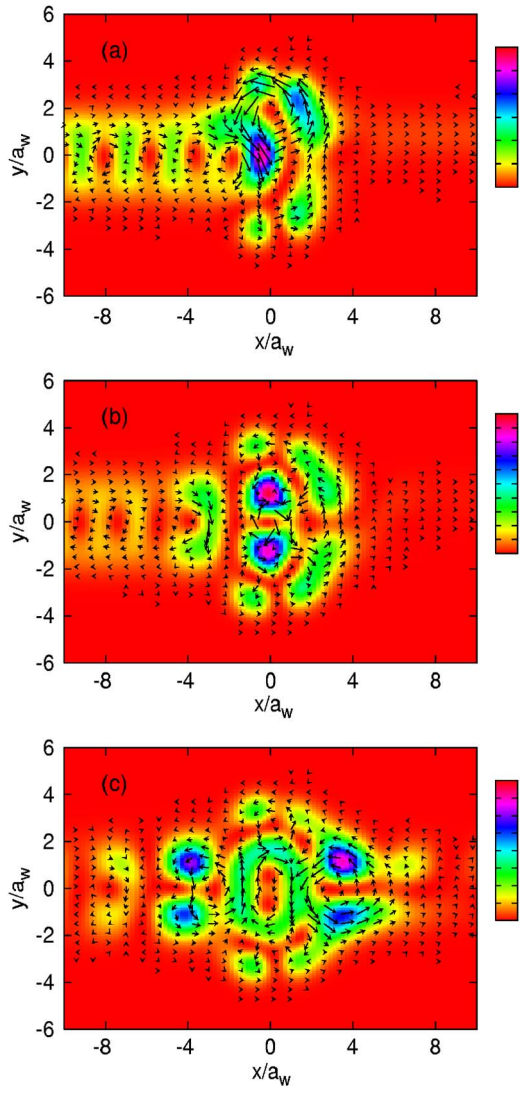

FIG. 5. (Color online) Probability density and electron current density (black arrows) for the case of $V_2=0$ meV and $B=0.5$ T at $X=$(a) 1.58; (b) 1.83; and (c) 1.97. Other parameters are $V_1=V_3=-6.0$ meV and $L=4.82a_w$.

$=1.0$ meV; (ii) at $X=1.14$ for $V_2=2.0$ meV; and (iii) at $X=1.17$ for $V_2=3.0$ meV. These dip structures correspond to electrons coupled with higher probability to the LD forming a holelike state, and then being backscattered to the left lead resulting in a significant conductance dip.

In the mediate-KE single-mode regime, there is a hump structure in G except for the case of $V_2=1.0$ meV. The broad nature of these structures implies the short electron dwell time of the quasibound states in the UD. To probe this transport mechanism, we plot the probability density and electron current density in real space shown in Fig. 4. Without a central barrier, the electrons are easily coupled to the LD and then doing cyclotron motion coupled backward with alignment to the second quasibound state in the UD resulting in a resonant transmission [see Fig. 4(a)]. For $V_2=1.0$ meV such an alignment in energy disappears, as a result no hump structure can be found. When the strength of the central barrier increases [see Figs. 4(b) and 4(c)], the electron energy is gradually allowed to align to the first quasibound state energy in the UD to facilitate a resonant transmission. It is interesting to mention that for the case of $V_2=0$ meV the shoulder of the hump structure at $X=1.58$ corresponds to a resonant transmission with lateral tunneling through the central barrier weakly coupling to the LD as displayed in Fig. 5(a).

Now we turn to discuss the high-KE single-mode regime. The general transport characteristics are small peaks in G with height around $0.2G_0$. In this regime, electrons are allowed to be well-coupled to the LD in accompanying a pinning effect around the central barrier. For the case without a central barrier, the electrons at energy $X=1.83$ form a (1,2)-like quasibound state between the UD and the LD, as is shown in Fig. 5(b). The second small peak ($X=1.97$) in G corresponds to a mixed (2,2)-like quasibound state [see Fig.

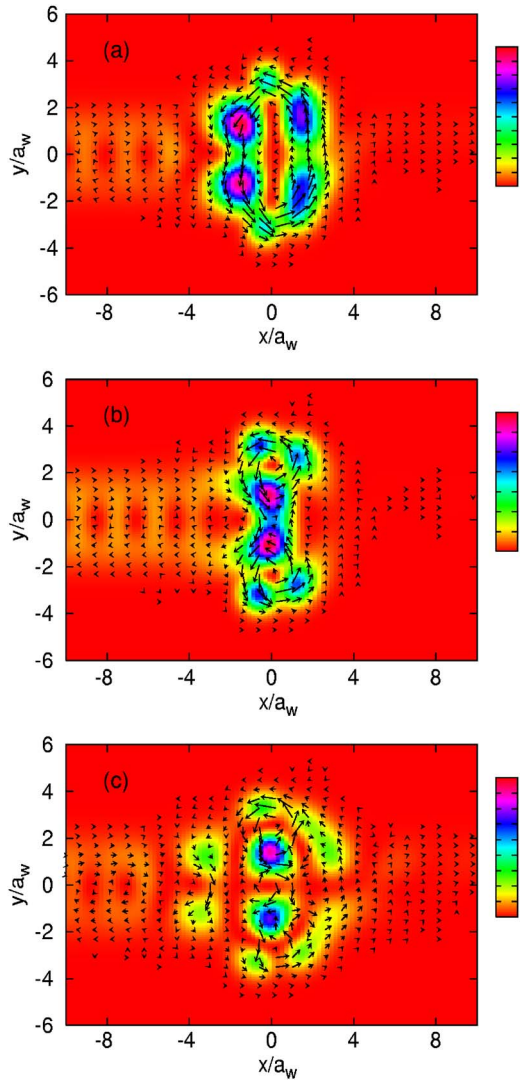

FIG. 6. (Color online) Probability density and electron current density (black arrows) for the case of $V_2=2.0$ meV and $B=0.5$ T at $X=$(a) 1.68; (b) 1.80; and (c) 1.91. Other parameters are the same as Fig. 5.

5(c)]. This state is constructed by four localized electronic cyclotron orbits—two stronger in front of and behind the central barrier and two weaker around the UD and the LD—to form an artificial *holelike quasibound state* between the parallel dots without a central barrier.

If we increase the height of the central barrier to $V_2=2.0$ meV, we find that there are three small resonant peaks in G at $X=1.68$, 1.80, and 1.91. Their corresponding transport patterns in real space are shown in Fig. 6. The first small peak at $X=1.68$ is a perfect (2,2)-like quasibound state[8] as demonstrated in Fig. 6(a). We note that there are two valley structures, on the sides of this resonant peak, with conductance minima at $X=1.66$ and 1.76. At these incident energies, the electrons only have good coupling to the UD due to the Lorentz force induced shifting effect. When the electrons are well-coupled to the whole DOQD system, such shifting effect becomes unimportant and the transport feature exhibits a clear resonant peak in G.

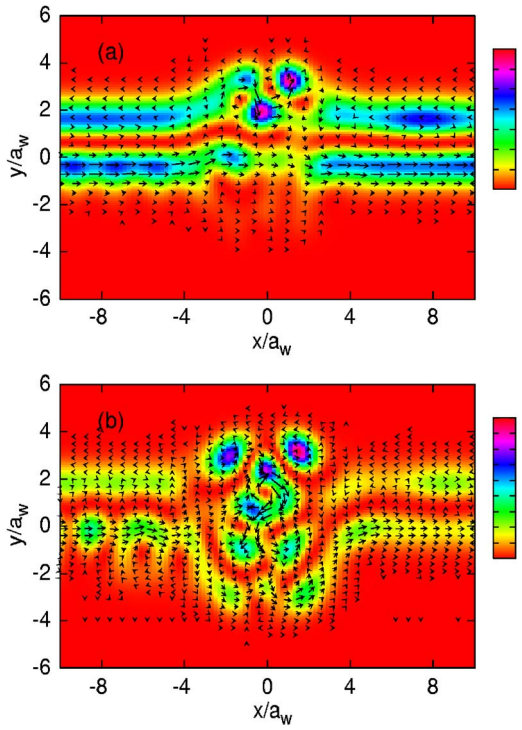

FIG. 7. (Color online) Probability density and electron current density (black arrows) for the case of $V_2=0$ meV and $B=0.5$ T at $X=$(a) 2.28 and (b) 2.51. Other parameters are $V_1=V_3=-6.0$ meV, $L=4.82a_w$, and incident mode $n=1$.

In Fig. 6(b), we show the electronic transport behavior at the second small peak ($X=1.80$). It is clearly seen that the counterclockwise cyclotron orbits are separated symmetrically by the central barrier. Due to the Lorentz force, the electrons are able to laterally tunnel through the central barrier spending more time on each side of the barrier thus forming a (1,2)-like quasibound state. With higher incident energy $X=1.91$, not only the tunneling feature of the UD-LD coupling is present, the electrons are also able to do cyclotron motion bypassing the central barrier [see Fig. 6(c)]. It is interesting to mention in passing that the small peaks at $X=1.61$, 1.71, and 1.87 for the case of $V_2=1.0$ meV as well as the small peaks at $X=1.73$, 1.86, and 1.94 for the case of $V_2=3.0$ meV have transport features similar to those of $V_2=2.0$ meV.

2. Double-mode regime

In contrast to the single-mode regime, one can find a conductance peak in the low-KE double-mode regime only for the case of $V_2=0$ meV at $X=2.01$ [see the solid curve in Fig. 2(a)]. This peak structure indicates a resonant transmission with coupling to the lowest quasibound state in the UD. For this case without a central barrier and in the mediate-KE double-mode regime, there are two small peak structures in G. First, a resonant transmission due to a magnetic Fabry-Pérot-type resonance in the upper open quantum dot in the upper incident channel is found at $X=2.28$ forming a resonant peak structure in G as is clearly demonstrated in Fig. 7(a). The electrons in the lower channel transport directly

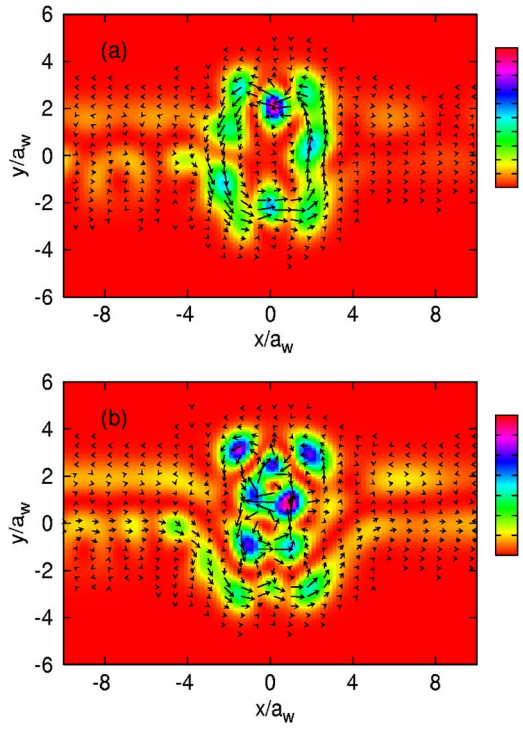

FIG. 8. (Color online) Probability density and electron current density (black arrows) for the case of $V_2=1.0$ meV and $B=0.5$ T at $X=$(a) 2.31 and (b) 2.56. Other parameters are the same as Fig. 7.

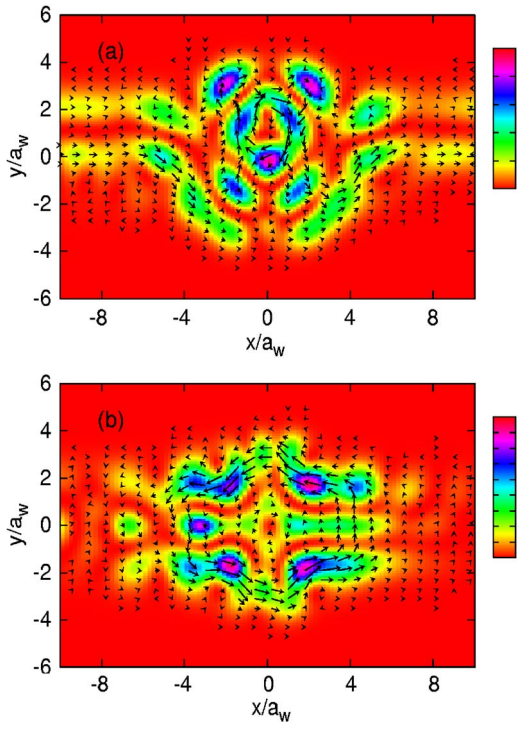

FIG. 9. (Color online) Probability density and electron current density (black arrows) for the case of $V_2=1.0$ meV in the high-KE double-mode regime in a magnetic field $B=0.5$ T at $X=$(a) 2.86 and (b) 2.96. Other parameters are $V_1=V_3=-6.0$ meV, $L=4.82a_w$, and incident mode $n=1$.

through the DOQD system with coupling to the upper channel. On the other hand, electrons with incident energy $X=2.51$ manifest a smaller peak structure in G that implies a short-lived resonant state. Figure 7(b) shows that the transport mechanism of this small peak structure is nontrivial: The electrons can form a (2,1)-like quasibound state in the UD with *magnetic turbulence* in the central part of the wire and weakly coupling to the LD. A more complicated magnetic turbulence feature can be found if electrons are incident from the first mode ($n=0$), due to their higher electron kinetic energy.

Contrarily, for $V_2=1.0$ meV in the mediate-KE double-mode regime, there are two small dip structures in G at $X=2.31$ and 2.56. First, the electrons with incident energy $X=2.31$ prefer to do a round trip motion around the central barrier forming a strong UD-LD coupling to construct a perfect quasibound state in the parallel DOQD system as depicted in Fig. 8(a). In addition, a weaker peak is found at $X=2.56$ indicating a shorter living quasibound state. Indeed, as shown in Fig. 8(b), both the probability density and the electron current density are complicated indicating a mixed resonant feature in transport. A resonant state is formed at the central part of the DOQD system with stronger coupling to the UD and weaker coupling to the LD due to the applied magnetic field in $\hat{\mathbf{z}}$ direction.

Now we turn to discuss the case of $V_2=1.0$ meV in the high-KE double-mode regime. There are two resonant features in G: A small sharp peak at $X=2.86$ and a deep sharp dip at $X=2.96$ [see the dashed curve in Fig. 2(a)]. The sharpness of the two structures implies a pure and long-lived resonant state. First, electrons with incident energy $X=2.86$ are able to construct a holelike resonant state at the upper central part of the parallel DOQD system as illustrated in Fig. 9(a). Specifically, the electrons have two channels incident from the left lead that can either couple to the LD or be backscattered to the UD. Those electrons transported through the LD can turn back due to the cyclotron motion and then couple to the UD. Again, electrons may be backscattered by the UD and then coupled to the central barrier. As such, the electrons construct a *magnetic holelike state* in the DOQD system. Second, the sharp dip in G at $X=2.96$ implies that a long-lived pure quasibound state is formed in the DOQD system. As shown in Fig. 9(b), the probability density shows a (2,3)-like quasibound state constructed in the system, and the weak link to the left and the right lead indicates the long dwell time of this resonant state. The electron current density forms a perfect circular motion around the parallel DOQD indicating a pure quasibound state.

Correspondingly, for the case of $V_2=0$ meV in the high-KE double-mode regime, there are two structures in G: a shallow dip at $X=2.78$ and a deep sharp dip at $X=2.93$ (see the solid curve in Fig. 2). The corresponding probability density and the electron current density distribution of these two resonance states are similar to the case of $V_2=1.0$ meV in the high-KE double-mode regime. However, unlike the small sharp peak in G at $X=2.86$ for the case of $V_2=1.0$ meV, electron transport with shallow dip in G at $X=2.78$ for the case of $V_2=0$ meV is not able to form a holelike bound state due to the absence of backscattering from the central barrier. Instead, an electron can form a quasibound state at the center

of the parallel DOQD system. The sharp dip in G at $X=2.93$ corresponds to a pure (2,3)-like quasibound state, which is similar to the dip structure at $X=2.96$ for the case of $V_2=1.0$ meV. The similarity of the transport features is due to the large loop of the symmetric cyclotron motion. Therefore the central barrier plays an insignificant role for such a transport feature. Furthermore, the three probability density peaks in the transverse direction imply that this (2,3)-like quasibound state is caused by the vicinity of the third subband threshold in the leads.

We now discuss the case of $V_2=2.0$ meV in the double-mode regime, there are three significant deep and sharp dips in G as displayed by the solid curve in Fig. 2(b). The first two sharp dips are at $X=2.35$ and 2.63 in the mediate-KE regime. First, for the case of the dip at $X=2.35$, the electrons make a perfect (2,1)-like quasibound state with clear cyclotron motion as demonstrated in Fig. 10(a). By tuning the central barrier and the energy of the incident electron to this condition, the UD and the LD can be strongly coupled with a long lifetime. Second, for the case of dip at $X=2.63$, the electron probability density forms a double ring structure in real space, and the electron current flows counterclockwise following this double ring loop with interference at the UD and the LD regions as is shown in Fig. 10(b). Such a resonant state formed around the central barrier is a quasibound state with negative binding energy −0.91 meV.[38] Turning to the very narrow and deep dip at $X=2.94$ in the high-KE double-mode regime, the electrons construct a very clear long-living state at the origin in real space as depicted in Fig. 10(c). The transport mechanism is that the electrons make intersubband transitions to the subband top at the origin of the central barrier forming a quasibound state. Two clear cyclotron orbits are seen in front of and behind the central barrier [see Fig. 10(c)].

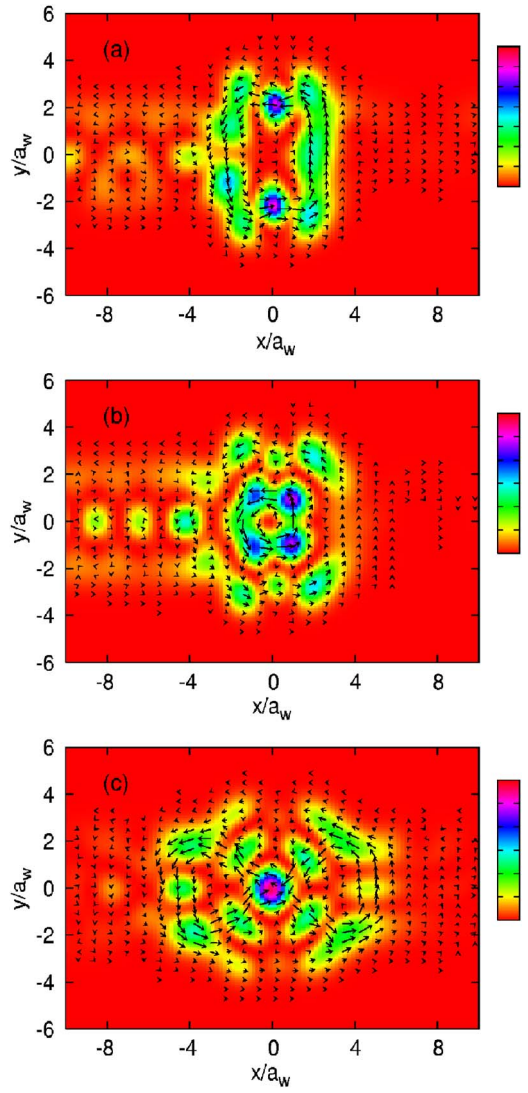

FIG. 10. (Color online) Probability density and electron current density (black arrows) for the case of $V_2=2.0$ meV in the double-mode regime at $X=$(a) 2.35; (b) 2.63; and (c) 2.94. Other parameters are $B=0.5$ T, $V_1=V_3=-6.0$ meV, $L=4.82a_w$, and incident mode $n=1$.

B. Tuning the magnetic field

Before we discuss the tuning effects on the coherent quantum transport by adjusting the strength of the external perpendicular magnetic field, we would like to mention that due to the complex potential-envelop nature of the laterally parallel DOQD system, there are several relatively short length scales of the system leading to the enhanced sensitivity to magnetic field in the range 0–1 T.

Figure 11 shows the magnetic field effects on the conductance to the DOQD system for an appropriate central barrier $V_2=2.0$ meV. The strength of the magnetic field is chosen to be $B=0.4$, 0.5, and 0.6 T, which correspond, respectively, to the effective magnetic length $a_w=30.59$, 29.34, and 29.10 nm; the effective subband separation $\hbar\Omega_w=1.22$, 1.32, and 1.44 meV; and the effective length of the DOQD system is $L/a_w=4.62$, 4.82, and 4.86. It is clearly shown in Fig. 11 that the conductance is essentially enhanced in the low-KE regime and suppressed in the high-KE regime. In the high-KE single-mode regime, the magnetic blocking effect is most significant for the case of $B=0.5$ T. However, in the double-mode regime, this blocking effect is significant for the case of $B=0.6$ T.

1. Single-mode regime

In the low-KE single-mode regime, there are three sharp downward dips in G at $X=1.18$ for $B=0.4$ T (solid), $X=1.14$ for $B=0.5$ T (dashed), and $X=1.09$ for $B=0.6$ T (dotted). The transport mechanism of these three dips is similar: The incident electron energy has good alignment to the discrete levels in the upper open dot forming a magnetic hole-like (2,1) quasibound state. For a weaker magnetic field $B=0.4$ T, the electrons with larger cyclotron orbit can bypass the central barrier, and hence the UD-LD coupling is strong enough to form a symmetric probability density pattern as is shown in Fig. 12(a). Therefore the conductance manifests a very sharp downward dip in response to this robust effect. When the magnetic field is further increased, the holelike quasibound state formed in the lower open dot is getting still weaker. This trend is clearly demonstrated in Figs. 12(b) and 12(c). For the case of $B=0.5$ T, the mediate UD-LD coupling leads to a clear Fano structure in the conductance [see the dashed curve in Fig. 11]. However, when the magnetic field is increased to $B=0.6$ T, the UD-LD coupling is further

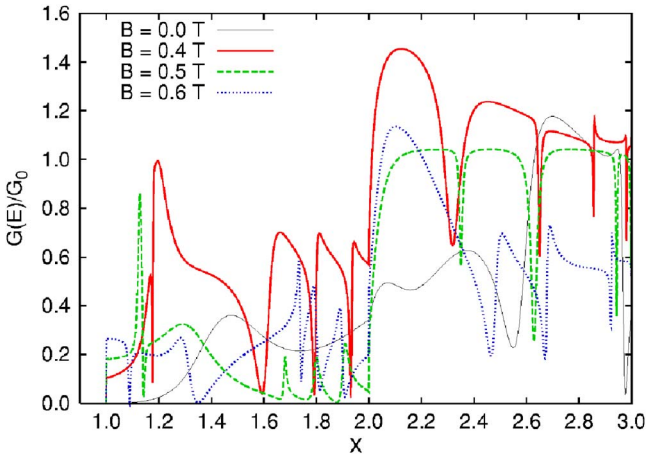

FIG. 11. (Color online) The conductance in units of $G_0=2e^2/h$ as a function of X for a DOQD system with central barrier $V_2=2.0$ meV in a magnetic field $B=$(a) 0.4 T (solid); (b) 0.5 T (dashed); and (c) 0.6 T (dotted). The conductance in the absence of magnetic field is plotted with a thin solid black curve for comparison. Other parameters are $V_1=V_3=-6.0$ meV and $L\simeq 141$ nm.

weaker leading to vanishing Fano structure and, instead, the electron conduction manifests a simple dip structure with zero conductance as depicted by the dotted curve in Fig. 11.

Turning to the mediate-KE single-mode regime, there are three significant resonant structures in G (see Fig. 11): The peak structure at $X=1.20$ for $B=0.4$ T, the hump structure at $X=1.29$ for $B=0.5$ T, and the valley structure at $X=1.35$ for $B=0.6$ T. First, the transport mechanism of the peak structure (for $B=0.4$ T) is related to the dip structure shown in Fig. 13(a) forming a Fano-like line shape. This peak structure is due to electrons with strong coupling to the upper open dot forming a holelike (2,1) quasibound state and making resonant transmission [see Fig. 13(a)]. Unlike the dip structure at $X=1.18$, there is almost no coupling to the lower open dot thus facilitating electron conduction, as coupling to the LD usually enhances backscattering to the left lead. Second, concerning the hump structure for the case of $B=0.5$ T, the energy alignment to the upper open dot is not present. Hence the electrons are not easily coupled to the parallel DOQD system. Instead, the electrons form a short-lived quasibound state in front of the central barrier as illustrated with Fig. 13(b). Third, for the case of valley structure at $X=1.35$ for $B=0.6$ T, an electron impinging on the central barrier could couple to the UD. In addition, the electron can make multiple cyclotron scattering between the two quasibound states formed on the two edges of the central barrier, which may backward tunnel through the central barrier exhibiting a zero conductance at $X=1.35$ (see the dotted curve in Fig. 11). The probability density and current density pattern is similar to Fig. 13(b) but with clearer cyclotron motion and a stronger quasibound state feature.

It is interesting to mention in passing that, in the mediate-KE single mode-regime, a holelike quasibound state is constructed in the upper open quantum dot for the case of $B=0.4$ T. When the magnetic field is increased to 0.5 T, such a holelike state has vanished. However, for a stronger magnetic field $B=0.6$ T, the holelike quasibound state appears again with significant magnetic multiple scattering on the two edges of the parallel DOQD system.

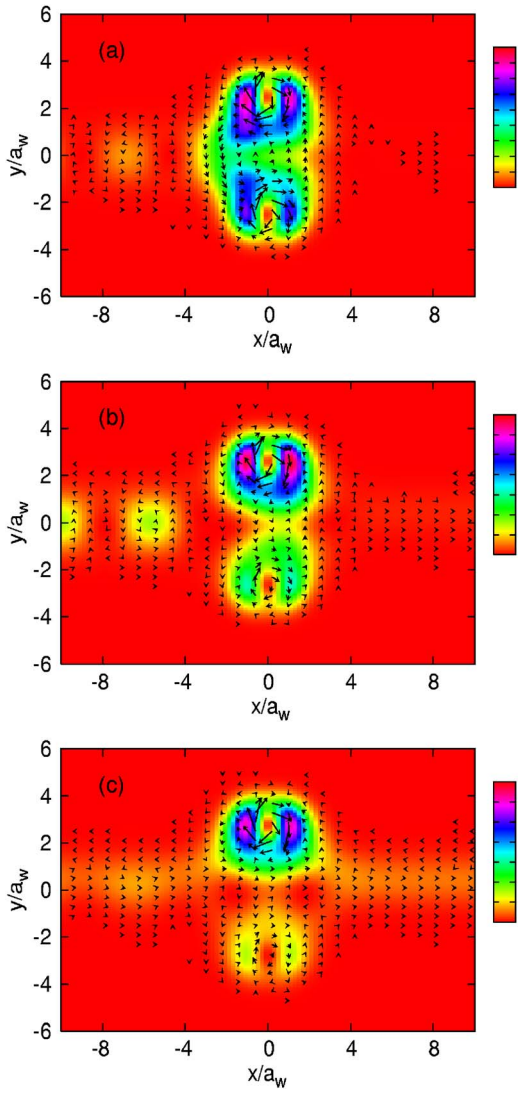

FIG. 12. (Color online) Probability density and electron current density (black arrows): (a) at $X=1.18$ for $B=0.4$ T; (b) at $X=1.14$ for $B=0.5$ T; and (c) at $X=1.09$ for $B=0.6$ T. Other parameters are $V_2=2.0$ meV, $V_1=V_3=-6.0$ meV, and $L\simeq 141$ nm.

For the case of $B=0.4$ T in the higher-KE single-mode regime, the conductance manifests strong oscillation effects as shown by the solid curve of Fig. 11. A clear broad dip structure is found at $X=1.59$, the electrons incident at this energy are scattered by the central barrier but can perform a big cyclotron orbit through the system with UD-LD coupling and construct a quasibound state in front of the central barrier. On the other hand, those electrons that are backscattered by the central barrier may interplay with the incident electrons constructing a holelike quasibound state in front of the central barrier. In Fig. 11, the sharp downward dips at $X=1.79$ and 1.93 for the case of $B=0.4$ T have similar probability and electron current density patterns to, respectively, the small peaks at $X=1.80$ and 1.91 for the case of $B=0.5$ T [see Figs. 6(b) and 6(c)]. When the magnetic blocking effect is significant, the electronic transport manifests

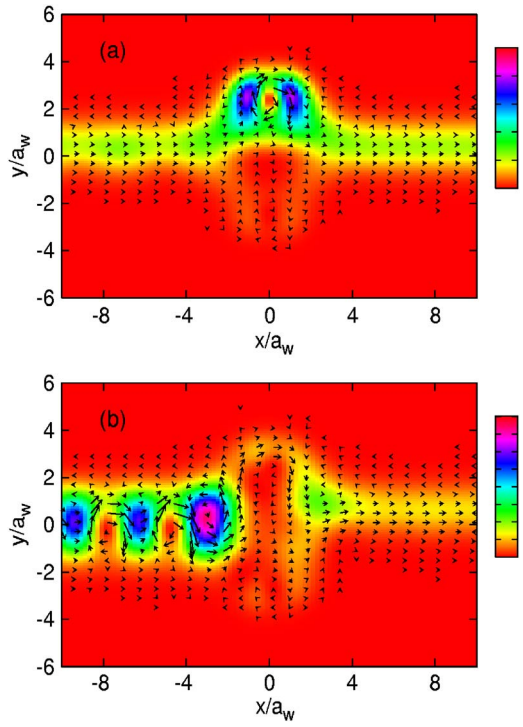

FIG. 13. (Color online) Probability density and electron current density (black arrows): (a) at $X=1.20$ for $B=0.4$ T; and (b) at $X=1.29$ for $B=0.5$ T. Other parameters are $V_2=2.0$ meV, $V_1=V_3=-6.0$ meV.

resonant transmission. However, if the magnetic blocking effect is insignificant, the transport feature tends to be resonant reflection.

For the case of a higher magnetic field $B=0.6$ T, the conductance manifests three Fano line shapes in the high-KE single-mode regime. The transport features for the Fano dips at $X=1.74$, 1.81, and 1.91 are very similar to, respectively, the three small dips at $X=1.68$, 1.80, and 1.91 for the case of $B=0.5$ T T, as is shown in Fig. 6. The transport features of the Fano peaks at $X=1.79$ and 1.89 are similar to their Fano dips but with stronger coupling to the right lead. However, the transport feature of the first Fano peak at $X=1.73$ has a significant difference with its corresponding Fano dip at $X=1.74$. The probability density and the electron current density pattern of the Fano peak is shown in Fig. 14. The electrons construct a (2,2)-like quasibound state between the UD and the central barrier. In addition, the electrons can also couple to the LD forming a complete cyclotron motion in the whole DOQD system. The weak coupling to the two leads shown in Fig. 14 implies the long dwell time of this quasibound state.

2. Double-mode regime

Now we turn to study the transport features in the double-mode regime. In this regime, the conductance manifests significant downward-dip structures implying resonant reflection. For the case of $B=0.4$ T in the mediate-KE regime, there are two significant dip structures in G at $X=2.32$ and 2.55 as shown by the solid curve in Fig. 11. When the electrons are incident with energy $X=2.32$, the wave function scars are found not only in the DOQD but also in the left lead as is shown in Fig. 15(a), this indicates that a strong quantum interference occurs between two propagating channels in the left lead. Moreover, this quantum interference occurring in the lead also implies a metastable quasibound state with a short dwell time, and hence the conductance manifests a broad-dip feature. Furthermore, a strong dot-lead coupling can be found by the high probability density on the left edge of the DOQD system. When the electrons are incident with higher energy $X=2.65$, they can construct a perfect (2,4)-like quasibound state in the parallel DOQD system, as is shown in Fig. 15(b). In addition, this quasibound state can easily couple to the upper and the lower open dot thus ac-

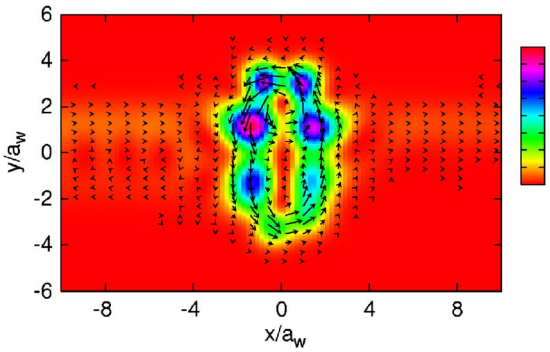

FIG. 14. (Color online) Probability density and electron current density (black arrows) for the case of $B=0.6$ T at $X=1.73$. Other parameters are $V_2=2.0$ meV and $V_1=V_3=-6.0$ meV.

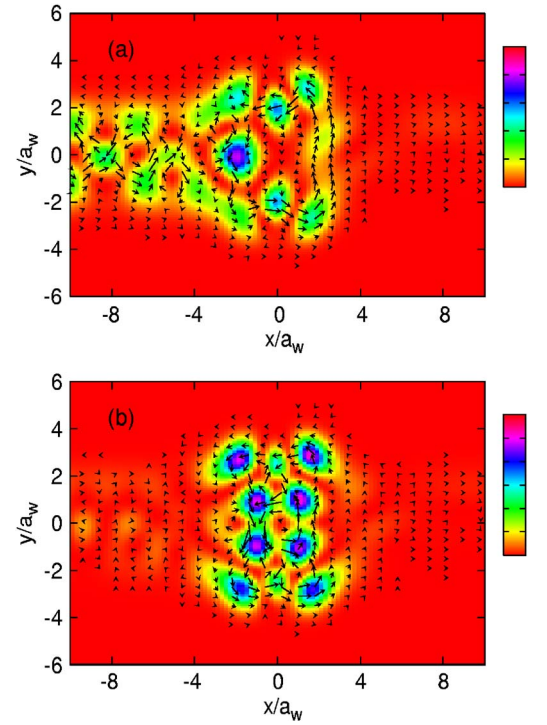

FIG. 15. (Color online) Probability density and electron current density (black arrows) for the case of $B=0.4$ T in the mediate-KE double-mode regime at $X=$(a) 2.32 and (b) 2.65. Other parameters are $V_2=2.0$ meV, $V_1=V_3=-6.0$ meV, and incident mode $n=1$.

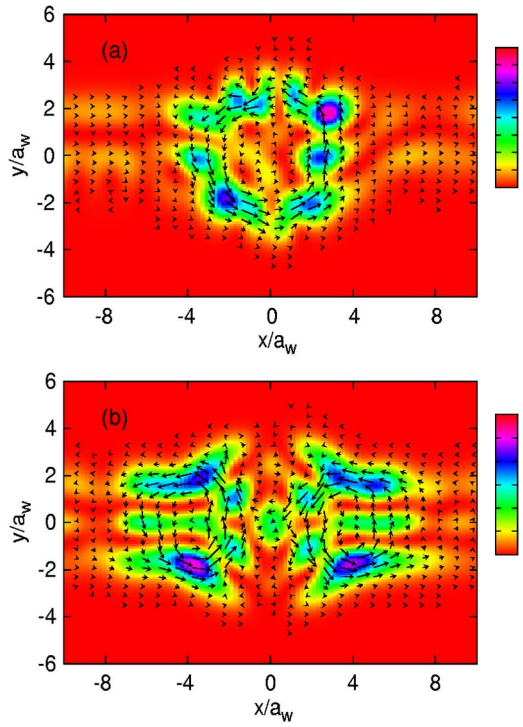

FIG. 16. (Color online) Probability density and electron current density (black arrows) for the case of $B=0.4$ T in the high-KE double-mode regime at $X=$(a) 2.85 and (b) 2.98. Other parameters are $V_2=2.0$ meV, $V_1=V_3=-6.0$ meV, and incident mode $n=1$.

complishing a highly symmetric probability pattern.

For the case of $B=0.4$ T in the high-KE double-mode regime, there are two narrow sharp dips in G at $X=2.85$ and 2.98 (see the solid curve in Fig. 11). When the electrons are incident with energy $X=2.85$, the electrons have a strong coupling to the parallel DOQD system forming a (2,3)-like quasibound state, and this state has weak coupling to the UD and the LD, as depicted in Fig. 16(a). If the electrons are incident with energy $X=2.98$, the conductance feature is a very sharp and narrow dip. The electrons can perform intersubband transitions to the threshold of the third subband forming a quasibound state in the left and the right lead as is clearly demonstrated in Fig. 16(b). The two clear cyclotron orbits in front of and behind the DOQD system are found with inversion symmetry implying a long-lived quasibound state. Due to the Lorentz force, such a state formed in the lead may flow back to the system forming (1,2)-like metastable quasibound states either in front of or behind the central barrier, and these two metastable states may have weak coupling through the central barrier.

For the case of $B=0.6$ T in the double-mode regime, the transport characteristics exhibit asymmetric dip features in the conductance as is shown by the dotted curve in Fig. 11. These dips are at $X=2.47$, 2.67, and 2.92 with an opening line shape in the low-energy part of the dip structure and with an abrupt change in G in the high-energy part of the dip structure. The transport features of the three significant asymmetric dips are displayed in Figs. 17(a)–17(c). The general transport features of these asymmetric dips are related to the "quantum peg" effect.[38]

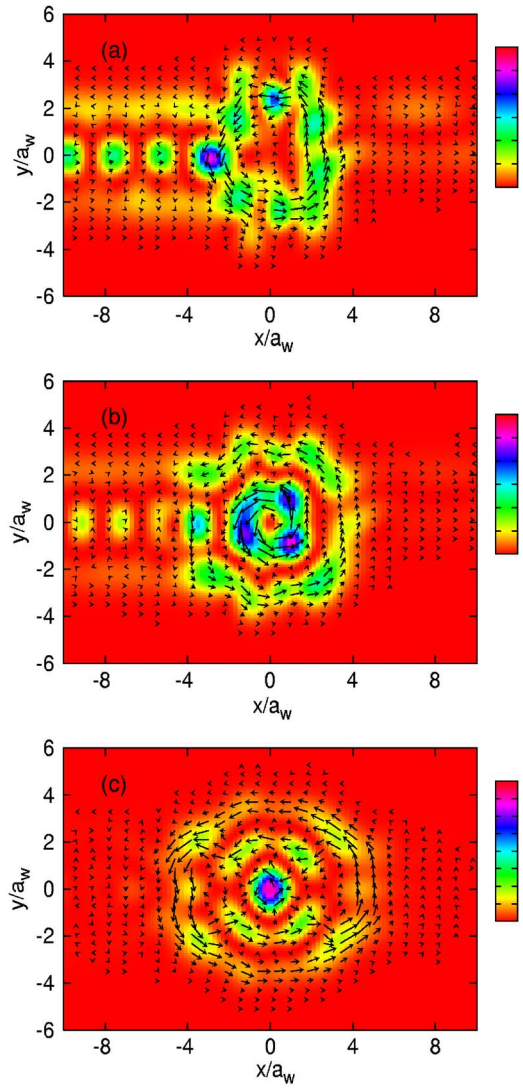

FIG. 17. (Color online) Probability density and electron current density (black arrows) for the case of $B=0.6$ T in the double-mode regime at $X=$(a) 2.47; (b) 2.67; and (c) 2.92. Other parameters are $V_2=2.0$ meV, $V_1=V_3=-6.0$ meV, and incident mode $n=1$.

The electrons with incident energy $X=2.47$ perform a cyclotron-type multiple scattering in the DOQD system with strong constructive quantum interference with incident electron waves on the left edge of the system as is shown in Fig. 17(a). For a higher incident electron energy $X=2.67$, the cyclotron-type quasibound state has a longer dwell time and the probability pattern displays a double-ring structure. It is clearly demonstrated in Fig. 17(b) that a "quantum peg" structure in real-space probability density is constructed around the central barrier (a quasibound state with negative binding energy). When the incident electron energy is further raised to $X=2.92$, one can find not only the double-ring structure but also a probability density peak at the origin of the central barrier as is depicted in Fig. 17(c).

The electron current flows dominantly through the outer ring-shaped path indicating a perfect quasibound state constructed around the whole system with long lifetime. When the electrons flow through the outer ring-shape path and

close to the UD or the LD, they may couple to the dot or turn to couple to the inner ring-shaped state. The low probability density in the UD and the LD implies the electrons traverse directly through the dots. On the other hand, those electrons coupled to the inner path may make intersubband transitions to a localized subband top formed at the origin of the central barrier trapped temporarily forming a quasibound state. This feature is an indirect intersubband transition mechanism similar to the case of $B=0.5$ T at $X=2.94$ as is shown in Fig. 10(c).

It is also worth to point out that for the case of $B=0.6$ T in the double-mode regime, the asymmetric dip structure at $X=2.92$ is narrower then the other two dips at lower energies, which in reality forms a Fano-type line shape. The Fano peak at $X=2.93$ has a probability density and electron current density pattern similar to its corresponding Fano-dip at $X=2.92$, but with stronger coupling to the right lead. The Fano effect is found to be prominent at the same specific magnetic fields such as $B=0.6$ T, while it is not distinct in the other values. This implies that the coherence nature of the quantum transport through the laterally parallel DOQD system strongly depends on the magnetic field.

IV. CONCLUSIONS

We have demonstrated tunable transport effects of coupling modes in laterally parallel double open quantum dots. In general the applied perpendicular homogeneous magnetic field plays a blocking effect on the quantum transport through the parallel DOQD system. Due to the complex potential-envelop nature of the system, there are several relatively short length scales leading to the sensitivity to magnetic field.

By tuning the central barrier, we have found Fano-type line shapes in the conductance in the low-KE single-mode regime. The peaks of these Fano-type line shapes are magnetic holelike quasibound-state features in the upper open quantum dot. In the mediate-KE single-mode regime, resonant coupling to the upper open dot is determined by the energy alignment of the incident electron energy with the quasibound levels in the upper quantum dot. In the high-KE single-mode regime, an interesting holelike quasibound-state feature has been found in the absence of a central barrier by tuning the incident electron energy just below the second subband threshold. Moreover, we have demonstrated the robust features of tunneling through and bypassing the central barrier in the transverse direction to achieve the UD-LD coupling.

In the double-mode regime, we have found a magnetic Fabry-Pérot-type resonant transmission in the upper open dot if the incident kinetic energy is low. In the mediate-KE regime, we have demonstrated the possibility of the magnetic turbulence effect in the central part of the system in the absence of a central barrier. A magnetic holelike quasibound state feature has been found in the high-KE double-mode regime for a weak central barrier. A clear "quantum peg" structure can be found in the mediate-KE double-mode regime for the case of mediate central barrier. Moreover, in the high-KE double-mode regime, we have found a quasibound state induced by intersubband transitions to the subband top located at the origin of the central barrier.

By tuning the magnetic field, we have found a Fano to downward-dip line-shape crossover on the quantum transport in the low-KE single-mode regime. The magnetic field manipulated energy alignment effect to the upper open dot has also been demonstrated in the mediate-KE single-mode regime. In the high-KE single-mode regime, by increasing the magnetic field from 0.4 T to 0.5 T the conductance features change from downward dips, small peaks, to Fano line shapes.

In the double-mode regime, the effects of wave function scars and a clear (2,4)-like quasibound state feature have been found for the case of lower magnetic field in the mediate-KE regime. For this case, the electron transport with high-KE manifests a (2,3)-like state and a quasibound state trapped at the subband threshold in the leads. When the magnetic field is tuned to be higher ($B=0.6$ T), the dip structures in the conductance become asymmetric and the transport pattern changes to be "quantum peg" features. When the incident energy is just below the third subband threshold, we can find a robust quasibound state feature formed at the origin of the central barrier.

In summary, we have proposed a laterally parallel DOQD configuration for the investigation of tuning effects upon the coupling modes of lateral parallel quantum dots. Even for such a simple configuration, tuning the coupling modes by the central barrier or by the magnetic field has revealed an essentially complicated nature of coherent quantum transport.

ACKNOWLEDGMENTS

The authors acknowledge financial support by the Research and Instruments Funds of the Icelandic State, the Research Fund of the University of Iceland, and the Taiwan National Science Council. C.S.T. is grateful to the computational facility supported by the National Center for High-performance Computing in Taiwan.

[1] A. M. Chang, H. U. Baranger, L. N. Pfeiffer, and K. W. West, Phys. Rev. Lett. **73**, 2111 (1994).

[2] I. H. Chan, R. M. Clarke, C. M. Marcus, K. Campman, and A. C. Gossard, Phys. Rev. Lett. **74**, 3876 (1995).

[3] M. Persson, J. Pettersson, B. von Sydow, P. E. Lindelof, A. Kristensen, and K.-F. Berggren, Phys. Rev. B **52**, 8921 (1995).

[4] M. W. Keller, A. Mittal, J. W. Sleight, R. G. Wheeler, D. E. Prober, R. N. Sacks, and H. Shtrikmann, Phys. Rev. B **53**,

R1693 (1996).
[5] Y. Wang, N. Zhu, J. Wang, and H. Guo, Phys. Rev. B **53**, 16408 (1996).
[6] R. Akis, D. K. Ferry, and J. P. Bird, Phys. Rev. Lett. **79**, 123 (1997); **81**, 1745 (1998); J. P. Bird, R. Akis, D. K. Ferry, D. Vasileska, J. Cooper, Y. Aoyagi, and T. Sugano, *ibid.* **82**, 4691 (1999); A. P. S. de Moura, Y.-C. Lai, R. Akis, J. P. Bird, and D. K. Ferry, *ibid.* **88**, 236804 (2002).
[7] I. V. Zozoulenko and T. Lundberg, Phys. Rev. Lett. **81**, 1744 (1998).
[8] C. S. Tang, Y. H. Tan, and C. S. Chu, Phys. Rev. B **67**, 205324 (2003).
[9] A. A. Clerk, X. Waintal, and P. W. Brouwer, Phys. Rev. Lett. **86**, 4636 (2001).
[10] M. G. Vavilov, L. DiCarlo, and C. M. Marcus, Phys. Rev. B **71**, 241309(R) (2005).
[11] Y.-H. Kim, M. Barth, U. Kuhl, H.-J. Stöckmann, and J. P. Bird, Phys. Rev. B **68**, 045315 (2003).
[12] M. Mendoza and P. A. Schulz, Phys. Rev. B **71**, 245303 (2005).
[13] For a general overview see, e.g., W. G. van der Wiel, S. D. Franceschi, J. M. Elzerman, T. Fujisawa, S. Tarucha, and L. P. Kouwenhoven, Rev. Mod. Phys. **75**, 1 (2003).
[14] J. C. Chen, A. M. Chang, and M. R. Melloch, Phys. Rev. Lett. **92**, 176801 (2004).
[15] H. Lu, R. Lü, and B.-F. Zhu, Phys. Rev. B **71**, 235320 (2005); R. Lü, Z.-R. Liu, and G.-M. Zhang, cond-mat/0504288 (unpublished).
[16] G. Kießlich, P. Samuelsson, A. Wacker, and E. Schöll, cond-mat/0507403 (unpublished).
[17] T. H. Oosterkamp, T. Fujisawa, W. G. van der Wiel, K. Ishibashi, R. V. Hijman, S. Tarucha, and L. P. Kouwenhoven, Nature (London) **395**, 873 (1998).
[18] H. Jeong, A. M. Chang, and M. R. Melloch, Science **293**, 2221 (2001).
[19] N. Aoki, D. Oonishi, Y. Iwase, Y. Ochiai, K. Ishibashi, Y. Aoyagi, and J. P. Bird, Appl. Phys. Lett. **80**, 2970 (2002).
[20] T. Kostyrko and B. R. Bulka, Phys. Rev. B **71**, 235306 (2005).
[21] M. Elhassan, J. P. Bird, A. Shailos, C. Prasad, R. Akis, D. K. Ferry, Y. Takagaki, L.-H. Lin, N. Aoki, Y. Ochiai, K. Ishibashi, and Y. Aoyagi, Phys. Rev. B **64**, 085325 (2001).
[22] M. Elhassan, J. P. Bird, R. Akis, D. K. Ferry, T. Ida, and K. Ishibashi, J. Phys.: Condens. Matter **17**, L351 (2005).
[23] V. N. Stavrou and Xuedong Hu (unpublished).
[24] I. Zutić, J. Fabian, and S. Das Sarma, Rev. Mod. Phys. **76**, 323 (2004).
[25] R. Requist, J. Schliemann, A. G. Abanov, and D. Loss, Phys. Rev. B **71**, 115315 (2005).
[26] A. C. Johnson, C. M. Marcus, M. P. Hanson, and A. C. Gossard, Phys. Rev. B **71**, 115333 (2005).
[27] O. N. Jouravlev and Y. V. Nazarov, cond-mat/0507680 (unpublished).
[28] T. Kuzmenko, K. Kikoin, and Y. Avishai, Phys. Rev. Lett. **89**, 156602 (2002).
[29] U. Hartmann and F. K. Wilhelm, Phys. Rev. B **69**, 161309(R) (2004).
[30] G.-H. Ding, C. K. Kim, and K. Nahm, Phys. Rev. B **71**, 205313 (2005).
[31] I. V. Zozoulenko, A. S. Sachrajda, C. Gould, K.-F. Berggren, P. Zawadzki, Y. Feng, and Z. Wasilewski, Phys. Rev. Lett. **83**, 1838 (1999).
[32] V. Gudmundsson, Y. Y. Lin, C. S. Tang, V. Moldoveanu, J. H. Bardarson, and A. Manolescu, Phys. Rev. B **71**, 235302 (2005).
[33] V. Gudmundsson, G. Gudmundsdottir, J. H. Bardarson, I. Magnusdottir, C. S. Tang, and A. Manolescu, Eur. Phys. J. B **45**, 339 (2005).
[34] M. C. Rogge, F. Cavaliere, M. Sassetti, R. J. Haug, and B. Kramer, cond-mat/0507036 (unpublished).
[35] C. S. Chu and R. S. Sorbello, Phys. Rev. B **40**, 5941 (1989); P. F. Bagwell, *ibid.* **41**, 10354 (1990); S. A. Gurvitz and Y. B. Levinson, *ibid.* **47**, 10578 (1993).
[36] J. Faist, P. Guéret, and H. Rothuizen, Phys. Rev. B **42**, 3217 (1990).
[37] R. B. Laughlin, Phys. Rev. B **27**, 3383 (1983).
[38] V. Gudmundsson, C. S. Tang, and A. Manolescu, Phys. Rev. B **72**, 153306 (2005).
[39] C. S. Tang and C. S. Chu, Phys. Rev. B **53**, 4838 (1996); Physica B **254**, 178 (1998); Phys. Rev. B **60**, 1830 (1999); Physica B **292**, 127 (2000).
[40] J. F. Weisz and K.-F. Berggren, Phys. Rev. B **40**, 1325 (1989).
[41] S. A. Gurvitz, Phys. Rev. B **51**, 7123 (1995).
[42] U. Fano, Phys. Rev. **124**, 1866 (1961); U. Fano, Nuovo Cimento **12**, 156 (1935).